



HAL
open science

**Multiplicity dependence of jet-like two-particle
correlation structures in p–Pb collisions at
 $\sqrt{s_{NN}}=5.02\text{TeV}$**

B. Abelev, J. Castillo Castellanos, J. -L. Charvet, H. Borel, A.
Rakotozafindrabe, H. Pereira da Costa, For The Alice Collaboration

► **To cite this version:**

B. Abelev, J. Castillo Castellanos, J. -L. Charvet, H. Borel, A. Rakotozafindrabe, et al.. Multiplicity dependence of jet-like two-particle correlation structures in p–Pb collisions at $\sqrt{s_{NN}}=5.02\text{TeV}$. Physics Letters B, 2015, 741, pp.38 - 50. 10.1016/j.physletb.2014.11.028 . hal-01103913

HAL Id: hal-01103913

<https://hal.science/hal-01103913>

Submitted on 15 Jan 2015

HAL is a multi-disciplinary open access archive for the deposit and dissemination of scientific research documents, whether they are published or not. The documents may come from teaching and research institutions in France or abroad, or from public or private research centers.

L'archive ouverte pluridisciplinaire **HAL**, est destinée au dépôt et à la diffusion de documents scientifiques de niveau recherche, publiés ou non, émanant des établissements d'enseignement et de recherche français ou étrangers, des laboratoires publics ou privés.



Multiplicity dependence of jet-like two-particle correlation structures in p–Pb collisions at $\sqrt{s_{NN}} = 5.02$ TeV

ALICE Collaboration ^{*}

ARTICLE INFO

Article history:

Received 23 June 2014

Received in revised form 8 October 2014

Accepted 15 November 2014

Available online 20 November 2014

Editor: L. Rolandi

ABSTRACT

Two-particle angular correlations between unidentified charged trigger and associated particles are measured by the ALICE detector in p–Pb collisions at a nucleon–nucleon centre-of-mass energy of 5.02 TeV. The transverse-momentum range $0.7 < p_{T,assoc} < p_{T,trig} < 5.0$ GeV/c is examined, to include correlations induced by jets originating from low momentum-transfer scatterings (minijets). The correlations expressed as associated yield per trigger particle are obtained in the pseudorapidity range $|\eta| < 0.9$. The near-side long-range pseudorapidity correlations observed in high-multiplicity p–Pb collisions are subtracted from both near-side short-range and away-side correlations in order to remove the non-jet-like components. The yields in the jet-like peaks are found to be invariant with event multiplicity with the exception of events with low multiplicity. This invariance is consistent with the particles being produced via the incoherent fragmentation of multiple parton–parton scatterings, while the yield related to the previously observed ridge structures is not jet-related. The number of uncorrelated sources of particle production is found to increase linearly with multiplicity, suggesting no saturation of the number of multi-parton interactions even in the highest multiplicity p–Pb collisions. Further, the number scales only in the intermediate multiplicity region with the number of binary nucleon–nucleon collisions estimated with a Glauber Monte-Carlo simulation.

© 2014 The Authors. Published by Elsevier B.V. This is an open access article under the CC BY license (<http://creativecommons.org/licenses/by/3.0/>). Funded by SCOAP³.

1. Introduction

Data from p–Pb collisions at the LHC have resulted in several surprising measurements with observations which are typically found in collisions of heavy ions and are understood to be due to a collective expansion of the hot and dense medium (hydrodynamic flow). In particular, so-called ridge structures which span over a large range in pseudorapidity (η) have been observed in two-particle correlations [1–3]. Their modulation in azimuth is described by Fourier coefficients and is dominated by those of second (v_2) and third (v_3) order [2–4]. They are also found in the correlations of four particles [4,5] which are less sensitive to non-flow effects like resonance decays and jets. Evidence for the existence of a common flow velocity field has been further corroborated by particle-identification measurements of the same observables [6]. They revealed that the v_2 of pions, kaons and protons as a function of p_T shows a characteristic mass ordering as well as a crossing of pion and proton v_2 at about 2.5 GeV/c which is reminiscent of measurements in Pb–Pb collisions [7]. These findings hint at potentially novel mechanisms in collisions of small systems which are far from being understood theoretically. Several authors de-

scribe the results in the context of hydrodynamics [8–12], but also explanations in the framework of saturation models successfully describe some of the measurements [13,14].

While measurements of these correlations are suggestive of similarities between Pb–Pb and p–Pb collisions, measurements sensitive to energy loss in a hot and dense medium reveal no or minor modifications with respect to pp collisions. The inclusive hadron nuclear modification factor R_{pA} of minimum-bias p–Pb events shows no significant deviations from unity up to 20 GeV/c [15]. Measurements of the dijet transverse momentum imbalance show comparable results to simulated pp collisions at the same center-of-mass energy, independent of the forward transverse energy [16].

Towards a more complete picture of the physical phenomena involved in p–Pb collisions, it is interesting to study QCD interactions in the p_T range where these ridge-like structures have been observed. Parton scatterings with large transverse-momentum transfer ($Q^2 \gg \Lambda_{QCD}$, typically called *hard interactions*) lead to phenomena such as high- p_T jets. QCD-inspired models extrapolate these interactions to the low- p_T region where several such interactions can occur per nucleon–nucleon collision (multiple parton interactions – MPIs) and can hence contribute significantly to particle production [17,18]. The objective of the analysis presented in this paper is to investigate if jet-like structures

^{*} E-mail address: alice-publications@cern.ch.

in this low- p_T region show modifications as a function of event multiplicity in addition to the appearance of the ridge-like structures. The analysis employs two-particle azimuthal correlations within $|\eta| < 0.9$ from low to intermediate transverse momentum ($0.7 < p_T < 5$ GeV/c) in p-Pb collisions. After subtraction of the long-range pseudorapidity ridge-like structures, the yields of the jet-like near- and away-side peaks are studied as a function of multiplicity. As already shown in pp collisions, this analysis procedure allows the extraction of the so-called number of uncorrelated seeds, which in PYTHIA is proportional to the number of MPIs [19]. Thus the presented results allow to draw conclusions on the contribution of hard processes to particle production as a function of event multiplicity.

The paper is structured as follows: Section 2 presents the experimental setup followed by the event and track selections in Section 3 and the analysis details in Section 4. The results are presented in Section 5 followed by a summary.

2. Experimental setup

In the present analysis, p-Pb collision data at a centre-of-mass energy of $\sqrt{s_{NN}} = 5.02$ TeV collected by the ALICE detector in 2013 are used. The energies of the beams were 4 TeV for the proton beam and 1.58 TeV per nucleon for the lead beam. The nucleon-nucleon centre-of-mass system moves with respect to the ALICE laboratory system with a rapidity of -0.465 , i.e. in the direction of the proton beam. In the following, η denotes the pseudorapidity in the laboratory system.

A detailed description of the ALICE detector can be found in Ref. [20]. The subdetectors used in the present analysis for charged particle tracking are the Inner Tracking System (ITS) and the Time Projection Chamber (TPC), both operating in a solenoidal magnetic field of 0.5 T and covering a common acceptance of $|\eta| < 0.9$. The ITS consists of six layers of silicon detectors: two layers of Silicon Pixels Detectors (SPD), two layers of Silicon Drift Detectors and two layers of Silicon Strip Detectors, from the innermost to the outermost ones. The TPC provides tracking and particle identification by measuring the curvature of the tracks in the magnetic field and the specific energy loss dE/dx . The VZERO detector, which consists of two arrays of 32 scintillator tiles each, covers the full azimuth within $2.8 < \eta < 5.1$ (VZERO-A) and $-3.7 < \eta < -1.7$ (VZERO-C) and is used for triggering, event selection and event characterization. The trigger requires a signal of logical coincidence in both VZERO-A and VZERO-C. The VZERO-A, located in the flight direction of the Pb ions, is used to define event classes corresponding to different particle-multiplicity ranges. In addition, two neutron Zero Degree Calorimeters (ZDCs), located at 112.5 m (ZNA) and -112.5 m (ZNC) from the interaction point, are used for the event selection. The ZNA has an acceptance of 96% for neutrons originating from the Pb nucleus and the deposited energy is used as an alternative approach to define the event-multiplicity classes.

3. Event and track selection

The employed event selection [21] accepts 99.2% of all non-single-diffractive collisions. Beam-induced background is removed by a selection on the signal amplitude and arrival times in the two VZERO detectors. The primary vertex position is determined from the tracks reconstructed in the ITS and TPC as described in Ref. [22]. The vertex reconstruction algorithm is fully efficient for events with at least one reconstructed primary charged particle in the common TPC and ITS acceptance. Events with the coordinate of the reconstructed vertex along the beam axis z_{vtx} within 10 cm from the nominal interaction point are selected. About $8 \cdot 10^7$

events pass these event selection criteria and are used for the analysis.

The analysis uses charged-particle tracks reconstructed in the ITS and TPC with $0.2 < p_T < 5$ GeV/c within a fiducial region of $|\eta| < \eta_{max}$ with $\eta_{max} = 0.9$. The track selection is the same as in Ref. [2] and is based on selections on the number of space points, the quality of the track fit and the number of hits in the ITS, as well as the Distance of Closest Approach (DCA) to the reconstructed collision vertex. The track selection is varied in the analysis for the study of systematic uncertainties [2].

The efficiency and purity of the track reconstruction and the track selection for primary charged particles (defined as the prompt particles produced in the collision, including decay products, except those from weak decays of strange particles) are estimated from a Monte-Carlo simulation using the DPMJET version 3.05 event generator [23] with particle transport through the detector using GEANT3 [24] version 3.21. The efficiency and acceptance for track reconstruction is 68–80% for the p_T range 0.2–1 GeV/c, and 80% for $p_T > 1$ GeV/c with the aforementioned track selections. The reconstruction performance is independent of the p-Pb event multiplicity. The remaining contamination from secondary particles due to interactions in the detector material and weak decays decreases from about 5% to 1% in the p_T range from 0.5 to 5 GeV/c. The contribution from fake tracks, false associations of detector signals, is negligible. Corrections for these effects are discussed in Section 4. Alternatively, efficiencies are estimated using HIJING version 1.36 [25] with negligible differences in the results.

In order to study the multiplicity dependence of the two-particle correlations, the events are divided into classes defined according to the charge deposition in the VZERO-A detector (called VOA when referring to it as a multiplicity estimator). The events are classified in 5% percentile ranges of the multiplicity distribution, denoted as “0–5%” to “95–100%” from the highest to the lowest multiplicity.

The VZERO-A detector is located in the direction of the Pb beam and thus sensitive to the fragmentation of the Pb nucleus, and is used as default multiplicity estimator. Two other estimators are employed to study the behaviour of the two-particle correlations as a function of the η -gap between the detector used to measure the multiplicity and the tracking detectors. These are CL1, where the signal is taken from the outer layer of the SPD ($|\eta| < 1.4$), and ZNA, which uses the ZNA detector ($|\eta| > 8.8$). Due to the limited efficiency of the ZNA, results are only presented for the 95% highest-multiplicity events. These estimators select events with different ranges of multiplicity at midrapidity. While the VOA estimator selects event classes with on average about 5 to 69 charged particles within $|\eta| < 0.9$ and p_T larger than 0.2 GeV/c, the CL1 has a slightly larger range (about 2 to 78) and the ZNA has a smaller range (about 10 to 46).

The observables in this analysis are calculated for events with at least one particle with $p_T > 0.2$ GeV/c within $|\eta| < 0.9$. Monte-Carlo simulations show that this selection reduces the number of events compared to all inelastic events by about 2%. These events are concentrated at low multiplicity in the 80–100% multiplicity classes.

4. Analysis

The two-particle correlations between pairs of trigger and associated charged particles are expressed as the associated yield per trigger particle in a given interval of transverse momentum, for each multiplicity class. The associated per-trigger yield is measured as a function of the azimuthal difference $\Delta\phi$ (defined within $-\pi/2$ and $3\pi/2$) and of the pseudorapidity difference $\Delta\eta$. The

condition $p_{T, \text{assoc}} < p_{T, \text{trig}}$ between transverse momenta of trigger and associated particles is required.

The associated yield per trigger particle is defined as

$$\frac{1}{N_{\text{trig}}} \frac{d^2 N_{\text{assoc}}}{d\Delta\eta d\Delta\varphi} = S(\Delta\eta, \Delta\varphi) \cdot C(\Delta\eta, \Delta\varphi), \quad (1)$$

where N_{trig} is the total number of trigger particles in the event class and p_T interval. The signal distribution $S(\Delta\eta, \Delta\varphi) = 1/N_{\text{trig}} d^2 N_{\text{same}}/d\Delta\eta d\Delta\varphi$ is the associated yield per trigger particle for particle pairs from the same event. The correction factor C is defined as:

$$C(\Delta\eta, \Delta\varphi) = \frac{\tilde{B}(\Delta\eta)}{B(\Delta\eta, \Delta\varphi)}, \quad (2)$$

where B describes the pair acceptance and pair efficiency of the detector while \tilde{B} is the pair acceptance of a perfect but pseudorapidity-limited detector, i.e. a triangular shape defined by $\tilde{B}(\Delta\eta) = 1 - |\Delta\eta|/(2 \cdot \eta_{\text{max}})$. In this way, the resulting associated yields per trigger particle count only the particles entering the detector acceptance, as it is required for the definition of uncorrelated seeds, see below and the detailed discussion in Ref. [19].

$B(\Delta\eta, \Delta\varphi) = \alpha d^2 N_{\text{mixed}}/d\Delta\eta d\Delta\varphi$ is constructed by correlating the trigger particles in one event with the associated particles from different events in the same multiplicity class and within the same 2 cm-wide z_{vtx} interval (each event is mixed with about 5–20 events). It is normalized with a factor α which is chosen such that $B(\Delta\eta, \Delta\varphi)$ is unity at $\Delta\varphi = \Delta\eta \approx 0$ for pairs where both particles travel in approximately the same direction. The yield defined by Eq. (1) is constructed for each z_{vtx} interval to account for differences in pair acceptance and in pair efficiency. After efficiency correction (described below) the final per-trigger yield is obtained by calculating the average of the z_{vtx} intervals weighted by N_{trig} . A selection on the opening angle of the particle pairs is applied in order to avoid a bias due to the reduced efficiency for pairs with small opening angles. Pairs are required to have a separation of $|\Delta\varphi_{\text{min}}^*| > 0.02$ rad or $|\Delta\eta| > 0.02$, where $\Delta\varphi_{\text{min}}^*$ is the minimal azimuthal distance at the same radius between the two tracks within the active detector volume after accounting for the bending in the magnetic field.

Furthermore, correlations induced by secondary particles from neutral-particle decays are suppressed by cutting on the invariant mass (m_{inv}) of the particle pair. In this way pairs are removed which are likely to stem from a γ -conversion ($m_{\text{inv}} < 0.04$ GeV/ c^2), a K_s^0 decay ($|m_{\text{inv}} - m(K_s^0)| < 0.02$ GeV/ c^2) or a Λ decay ($|m_{\text{inv}} - m(\Lambda)| < 0.02$ GeV/ c^2). The corresponding masses of the decay particles (electron, pion, or pion/proton) are assumed in the m_{inv} calculation.

Each trigger and each associated particle is weighted with a correction factor that accounts for reconstruction efficiency and contamination by secondary particles. These corrections are applied as a function of η , p_T and z_{vtx} . The correction procedure is validated by applying it to simulated events and comparing the per-trigger pair yields with the input Monte-Carlo simulations. The remaining difference after all corrections (Monte-Carlo non-closure) is found to be negligible.

4.1. Long-range correlations subtraction

In addition to the jet-like peaks, ridge structures have been observed in p-Pb collisions [2,3]. These long-range structures are mostly independent of $\Delta\eta$ outside the jet-like peak and assumed to be independent below the peak and their modulation in azimuth is described by a Fourier expansion up to the third order. To study the properties of the jet-like peaks, these structures are subtracted.

On the near side ($-\pi/2 < \Delta\varphi < \pi/2$), the jet-like peak is centered around ($\Delta\eta = 0, \Delta\varphi = 0$), while the ridge structures extend to large $\Delta\eta$. Thus the near side is divided into short-range ($|\Delta\eta| < 1.2$) and long-range ($1.2 < |\Delta\eta| < 1.8$) correlations regions which are correctly normalized and subtracted from one another. Fig. 1 shows the $\Delta\varphi$ -distributions of the per-trigger yield in these two regions in the highest (0–5%) and lowest (95–100%) multiplicity classes.

On the away side ($\pi/2 < \Delta\varphi < 3\pi/2$) the jet contribution is also elongated in $\Delta\eta$. The jet and ridge contribution can therefore not be disentangled. As the ridge structures are mostly symmetric around $\Delta\varphi = \pi/2$ (the second Fourier coefficient is four times larger than the third coefficient [2,3]), the near-side long-range correlations are mirrored around $\Delta\varphi = \pi/2$ and subtracted from the away side (measured in $|\Delta\eta| < 1.8$). Also shown in Fig. 1 are the $\Delta\varphi$ -distributions of the symmetrized long-range correlations and the correlations after subtraction. Obviously, this symmetrization procedure does not account correctly for odd Fourier coefficients. To assess the effect of the third coefficient on the extracted observables, an additional $2v_3^2 \cos 3\Delta\varphi$ functional form is subtracted before the symmetrization. The v_3 is estimated as a function of multiplicity with the subtraction procedure described in Ref. [2]. The influence of the v_3 contribution is illustrated in the bottom left panel of Fig. 1. The effect of the symmetrization of the third Fourier component on the away-side yield amounts up to 4% and is a major contribution to the systematic uncertainties.

4.2. Observables

The event-averaged near-side, $\langle N_{\text{assoc, near side}} \rangle$, and away-side, $\langle N_{\text{assoc, away side}} \rangle$, per-trigger yields are sensitive to the fragmentation properties of low- p_T partons. They are calculated as the integral of the $\Delta\varphi$ projection of the long-range subtracted per-trigger yield (bin counting) respectively in the near-side and away-side peaks, above the combinatorial background. By definition after subtracting the long-range correlations ($1.2 < |\Delta\eta| < 1.8$) from the short-range one ($|\Delta\eta| < 1.2$), the baseline should be zero. Nevertheless, owing to minor differences between the detector efficiencies and those estimated with the Monte-Carlo simulations and a slight dependence of the single-particle distribution on η , a small residual baseline is present (about 0.003, hardly visible in Fig. 1), which is taken into account. Fig. 1 shows that the away-side peak is slightly wider than the near-side peak. Therefore, the near-side yield is evaluated in the region $|\Delta\varphi| < 1.48$ and the away-side yield in $|\Delta\varphi| > 1.48$. For the systematic uncertainty estimation, the value 1.48 has been varied by ± 0.09 .

Alternatively, the yields are also calculated with a fit method, using two Gaussians on the near side and one Gaussian on the away side superimposed on a constant baseline [19]. The differences between the results obtained with the two methods are included in the systematic uncertainties.

The average number of trigger particles depends on the number of parton scatterings per event as well as on the fragmentation properties of the partons. Therefore, the ratio between the number of trigger particles and the per-trigger yields is computed with the goal to reduce the dependence on fragmentation properties. This ratio, called average number of uncorrelated seeds, is defined for symmetric p_T bins as:

$$\begin{aligned} \langle N_{\text{uncorrelated seeds}} \rangle &= \frac{\langle N_{\text{trig}} \rangle}{\langle N_{\text{correlated triggers}} \rangle} \\ &= \frac{\langle N_{\text{trig}} \rangle}{1 + \langle N_{\text{assoc, near side}} \rangle + \langle N_{\text{assoc, away side}} \rangle}, \quad (3) \end{aligned}$$

where the correlated triggers are calculated as the sum of the trigger particle and the particles associated to that trigger parti-

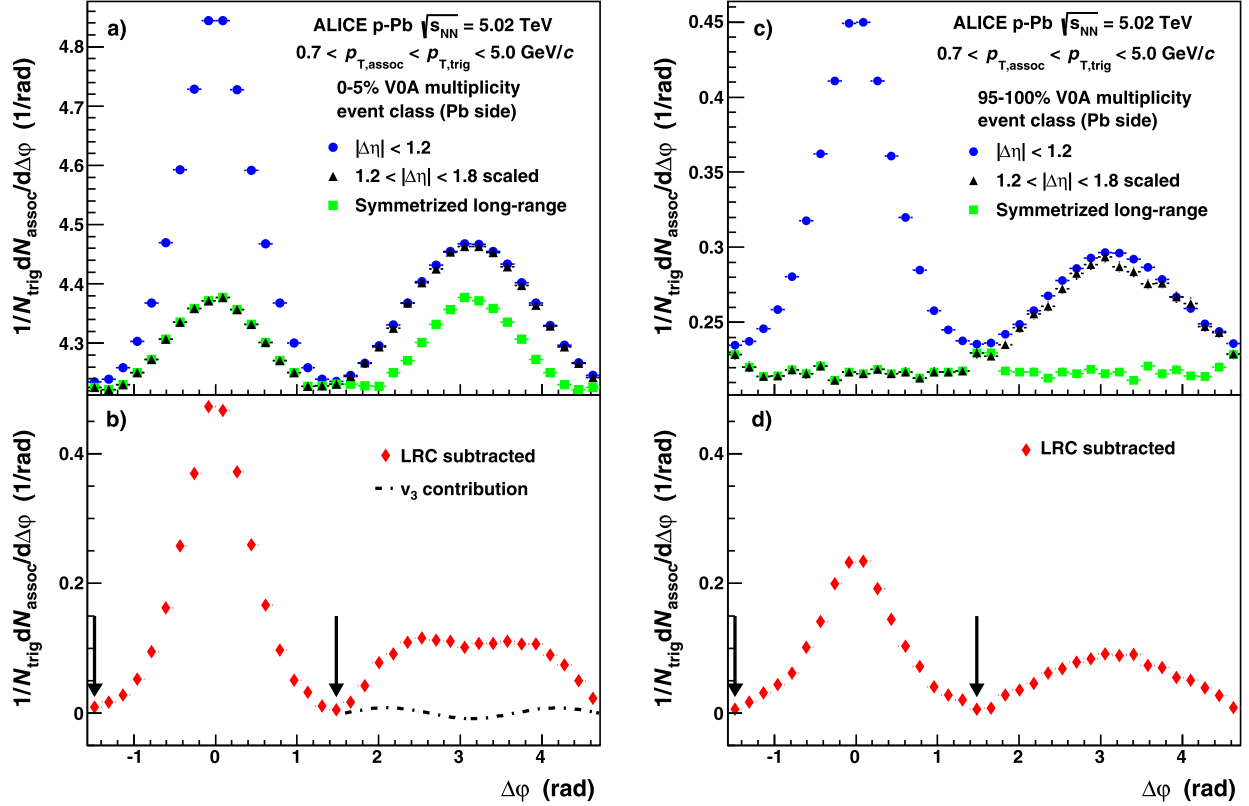


Fig. 1. Per-trigger yield as a function of $\Delta\phi$ with $0.7 < p_{T,assoc} < p_{T,trig} < 5$ GeV/c in the 0–5% event class (left) and 95–100% event class (right). The distributions show the correlations before subtraction (blue circles), the long-range correlations (black triangles) scaled according to the $\Delta\eta$ region in which they are integrated, the symmetrized near-side long-range correlations (green squares) and the correlations after long-range correlations (LRC) subtraction (red diamonds). The vertical arrows indicate the integration regions while the curve in the bottom left panel shows the magnitude of the third Fourier component on the away side. Statistical uncertainties are shown but are smaller than the symbol size. (For interpretation of the references to color in this figure, the reader is referred to the web version of this article.)

cle. In PYTHIA, for pp collisions [19], the uncorrelated seeds are found to be linearly correlated to the number of MPIs in a certain p_T range, independent of the η range explored. The selection $p_T > 0.7$ GeV/c has been found optimal since it is close to Λ_{QCD} and high enough to reduce contributions of hadrons at low p_T , e.g. from resonances and string decays.

4.3. Systematic uncertainties

Table 1 summarizes the systematic uncertainties related to the near-side and away-side long-range-subtracted yields extraction and to the uncorrelated seeds calculation. The largest uncertainty (5%) for the yields is due to the integration method estimated from the difference between bin counting and the fit. The v_3 -component estimation gives rise to an uncertainty only on the away side which is multiplicity-dependent. It is indicated by the range in the table where the largest value of 4% is obtained for the highest multiplicity. Other non-negligible uncertainties are due to the track selection (2%), the pile-up contamination (1%), estimated by excluding the tracks from different colliding bunch crossings, and the uncertainty on the tracking efficiency (3%) [15].

The total uncertainty for the yields is 6–8%, which translates into 3% uncertainty for the uncorrelated seeds where, owing to the definition, some uncertainties cancel. The total uncertainty is mostly correlated between points and between the different estimators.

5. Results

The near-side and away-side per-trigger yields are shown in Fig. 2 as a function of V0A multiplicity class for three different

Table 1
Summary of the systematic uncertainties. The uncertainties are independent of multiplicity, apart from the effect of the third Fourier component v_3 .

Source	Near-side yield	Away-side yield	Uncorrelated seeds
Bin counting vs. fit	5%	5%	1%
Baseline estimation	negl.	1%	negl.
v_3 component	0%	0–4%	0–1%
Track selection	2%	2%	negl.
Tracking efficiency	3%	3%	3%
Pile-up	1%	1%	negl.
MC closure	negl.	negl.	negl.
Event generator	negl.	negl.	negl.
Total	6%	6–8%	3%

p_T ranges. For the range $0.7 \text{ GeV/c} < p_{T,assoc} < p_{T,trig} < 5.0 \text{ GeV/c}$ (red triangles), the near-side (away-side) per-trigger yield increases from about 0.14 (0.08) in the lowest multiplicity class up to about 0.25 (0.12) at 60%, and it remains nearly constant from 60% to the highest multiplicity class.

The trigger particles can originate both from soft and hard processes, while the associated particles mostly belong to the mini-jets which originate from hard processes. Therefore, in the region where the associated yields per trigger particle show a plateau, the hard processes and the number of soft particles must exhibit the same evolution with multiplicity. This can be more easily understood with an example event containing N_{minijets} with N_{assoc} associated particles each and a background of N_{soft} particles with no azimuthal correlation. In this scenario, the associated yield per trigger-particle is:

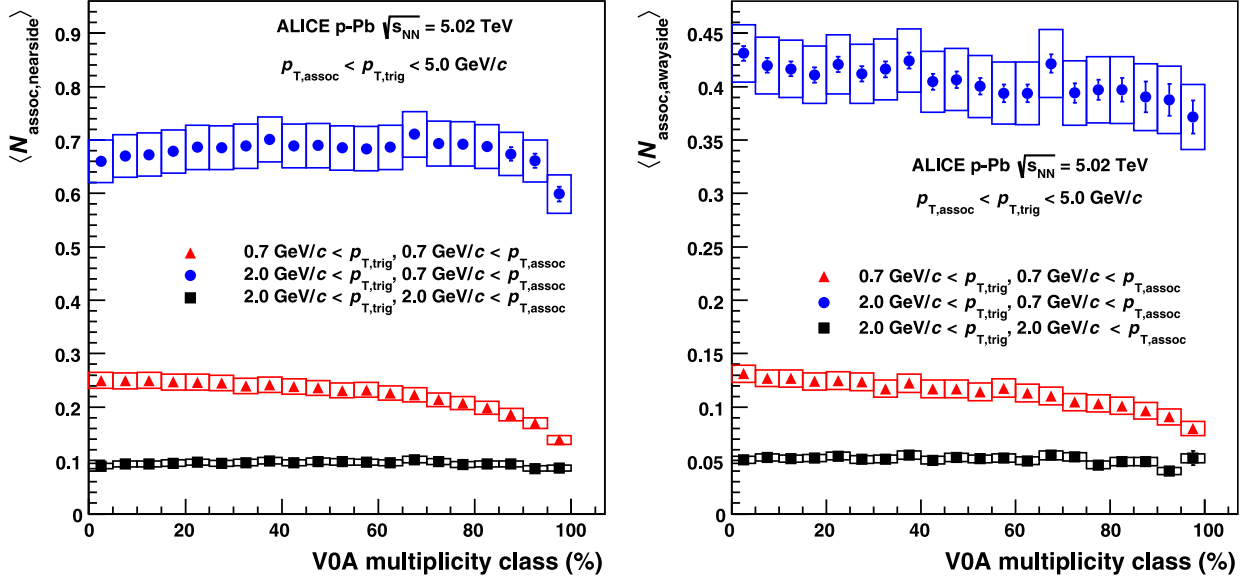


Fig. 2. Near-side (left panel) and away-side (right panel) per-trigger yields after long-range correlations subtraction as a function of VOA multiplicity class for several p_T cuts for trigger and associated particles: 0.7–5.0 GeV/c (red triangles), 0.7–5.0 GeV/c for $p_{T,\text{assoc}}$ and 2–5 GeV/c for $p_{T,\text{trig}}$ (blue circles) as well as 2–5 GeV/c (black circles). Statistical (lines) and systematic uncertainties (boxes) are shown, even though the statistical ones are mostly smaller than the symbol size. (For interpretation of the references to color in this figure, the reader is referred to the web version of this article.)

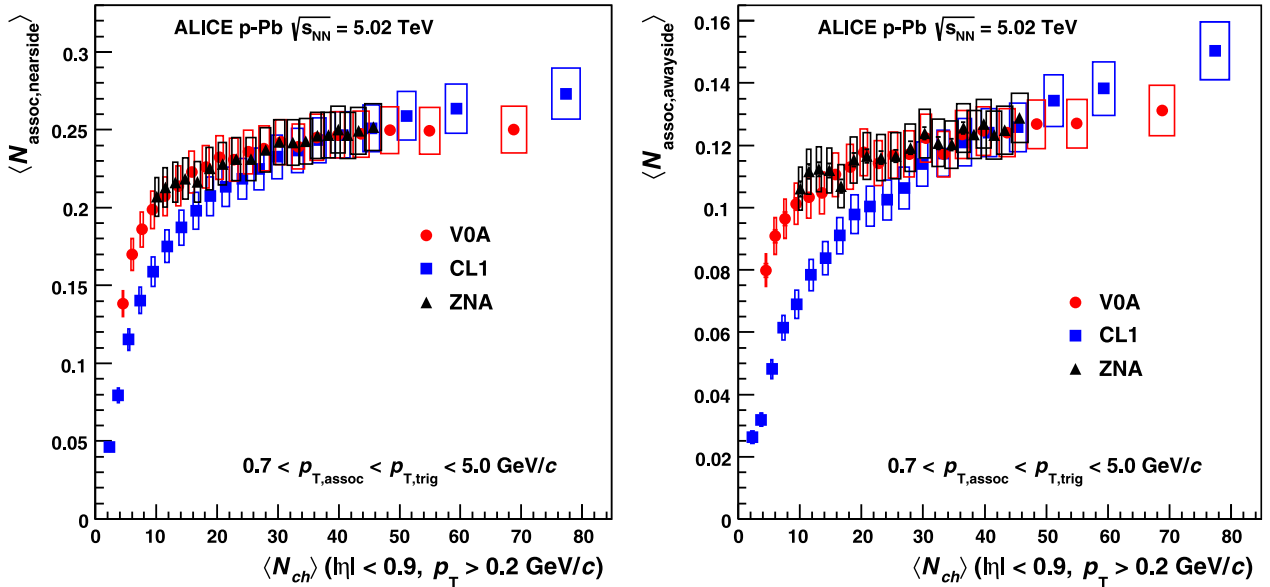


Fig. 3. Near-side (left panel) and away-side (right panel) per-trigger yields after long-range correlations subtraction as a function of the midrapidity charged particle multiplicity for the VOA (red circles), CL1 (blue squares) and ZNA (black triangles) multiplicity estimators. Statistical (lines) and systematic uncertainties (boxes) are shown, even though the statistical ones are smaller than the symbol size. (For interpretation of the references to color in this figure, the reader is referred to the web version of this article.)

$$\frac{\text{associated yield}}{\text{trigger particle}} = \frac{N_{\text{minijets}} \cdot N_{\text{assoc}}(N_{\text{assoc}} - 1)/2}{N_{\text{minijets}} \cdot N_{\text{assoc}} + N_{\text{soft}}}. \quad (4)$$

When the overall multiplicity, i.e. the denominator, changes, the fraction is constant if N_{minijets} (hard processes) and N_{soft} (soft processes) increase by the same factor. The given example can be easily extended to several events and to a different number of associated particles per minijet.

Increasing the p_T threshold of the trigger particles to 2 GeV/c (blue circles in Fig. 2), results in larger yields but with qualitatively the same multiplicity dependence. The plateau region extends in this case up to the 80% multiplicity class. Increasing also the threshold for the associated particles to 2 GeV/c (black squares)

reduces the yields while the plateau remains over a wide multiplicity range.

To compare results obtained with different multiplicity estimators, for each multiplicity class the average number of charged particles at midrapidity ($|\eta| < 0.9$) with $p_T > 0.2$ GeV/c has been computed. Fig. 3 shows the per-trigger yields in the near-side and in the away-side peaks as a function of the midrapidity charged particle multiplicity for the standard estimator VOA as well as for CL1 and ZNA. As discussed above, the multiplicity range covered by these estimators depends on the separation in pseudorapidity of the estimator and the tracking detector. The near-side (away-side) yields for VOA and ZNA show the same behaviour in the region between 10 and 45 charged particles in which their multiplicity

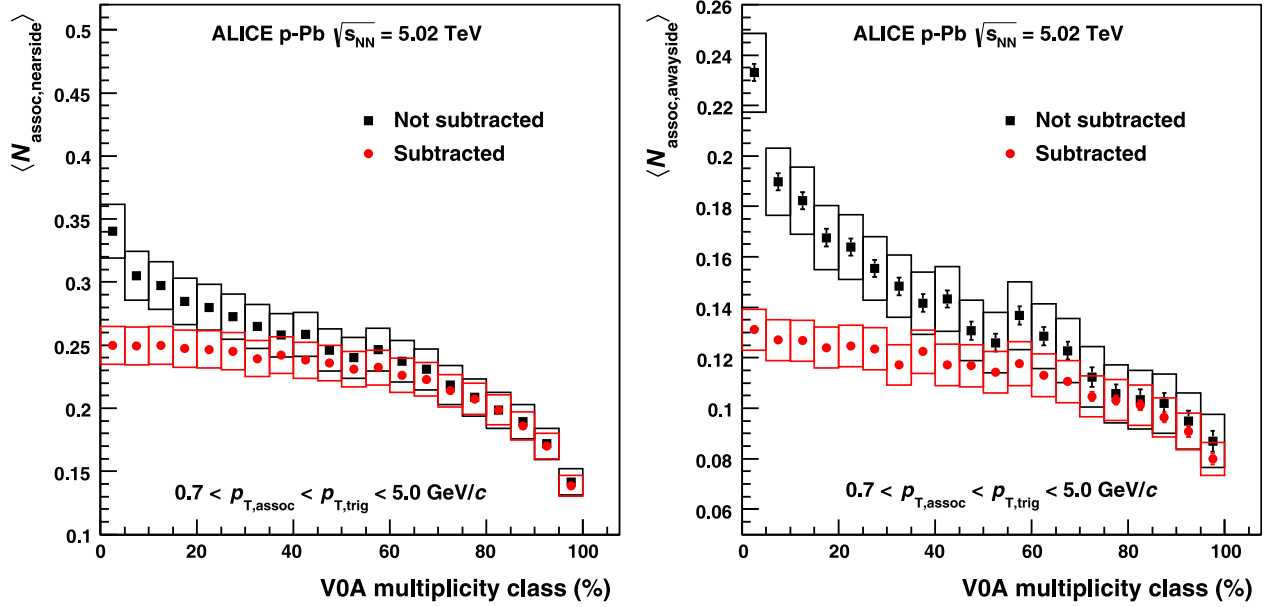


Fig. 4. Near-side (left panel) and away-side (right panel) per-trigger yields as a function of VOA multiplicity class with (red circles) and without (black squares) subtraction of the long-range correlations. Statistical (lines) and systematic uncertainties (boxes) are shown, even though the statistical ones are mostly smaller than the symbol size. (For interpretation of the references to color in this figure, the reader is referred to the web version of this article.)

range overlaps: a mild increase from about 0.2 (0.1) to about 0.25 (0.13). Below 10 charged particles, the yields for VOA decrease significantly to about 0.14 on the near side and 0.08 on the away side. The yields for CL1 exhibit a steeper slope than the two other estimators. This behaviour is expected from the event-selection bias imposed by the overlapping η -region of event selection and tracking: on the near side (away side) the value increases from about 0.04 to 0.27 (from about 0.02 to 0.15). The CL1 trends are qualitatively consistent with the results in pp collisions [19]. The overall behaviour for each estimator is similar when using higher p_T cuts for associated and trigger particles.

A key step of the analysis procedure is the subtraction of the long-range correlations. To assess the effect of this subtraction, a comparison between the yields with and without the ridge contribution has been performed. The determination of the yields in these two cases is, however, slightly different, since the non-subtracted distribution does not have a zero baseline by construction. In this case, the baseline is determined in the long-range correlations region ($1.2 < |\Delta\eta| < 1.8$) between the near-side ridge and the away-side peak at $1.05 < |\Delta\phi| < 1.22$.

The effect of the subtraction of the long-range correlations on the measured yields for the VOA estimator is presented in Fig. 4, where the near-side and away-side per-trigger yields with (red circles) and without (black squares) long-range correlations subtraction are shown. The yields agree with each other in the multiplicity classes from 50% to 100%, consistent with the observation that no significant long-range structure exists in low-multiplicity classes. For higher-multiplicity classes, a difference is observed: the near-side yield increases up to about 0.34 without the subtraction compared to about 0.25 with subtraction. On the away side the value is about 0.23 compared to 0.13. Thus, in the highest multiplicity class, the subtraction procedure removes 30–40% of the measured yields. The same observation is made for the other multiplicity estimators.

The conclusion drawn earlier, that the hard processes and the number of soft particles show the same evolution with multiplicity, is only valid when the long-range correlations structure is subtracted. This observation is consistent with a picture where the minijet-associated yields in p–Pb collisions originate from the inco-

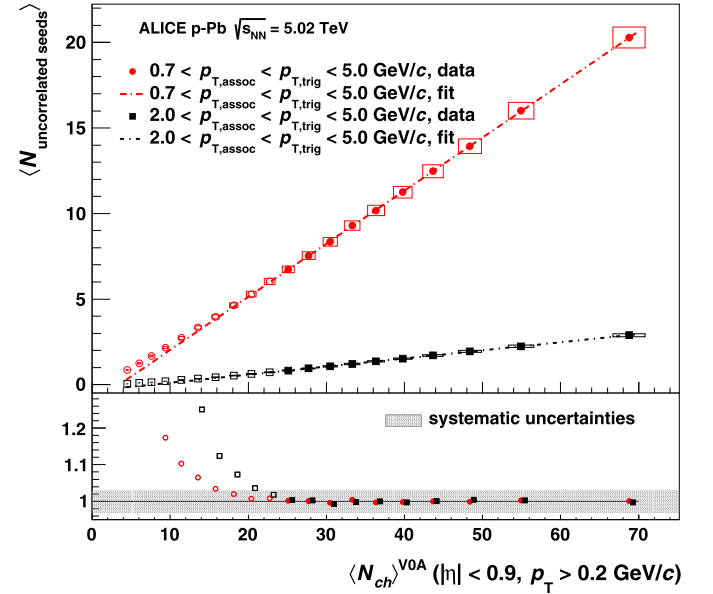


Fig. 5. Top panel: number of uncorrelated seeds as a function of the midrapidity charged particle multiplicity. Shown are results for two p_T cuts: $0.7 \text{ GeV}/c < p_{T,\text{assoc}} < p_{T,\text{trig}} < 5.0 \text{ GeV}/c$ (red circles) and $2.0 \text{ GeV}/c < p_{T,\text{assoc}} < p_{T,\text{trig}} < 5.0 \text{ GeV}/c$ (black squares). Each of them is fit with a linear function in the 0–50% multiplicity classes; open symbols are not included in the fit. Statistical (lines) and systematic uncertainties (boxes) are shown, even though the statistical ones are smaller than the symbol size. Bottom panel: ratio between the number of uncorrelated seeds and the linear fit functions. Black points are displaced slightly for better visibility. (For interpretation of the references to color in this figure, the reader is referred to the web version of this article.)

herent fragmentation of multiple parton–parton scatterings, while the long-range correlations appear unrelated to minijet production.

While the yields give information about the particles produced in a single parton–parton scattering, the uncorrelated seeds calculation (Eq. (3)) provides the number of independent sources of particle production. The uncorrelated seeds are proportional to the number of MPIs in PYTHIA.

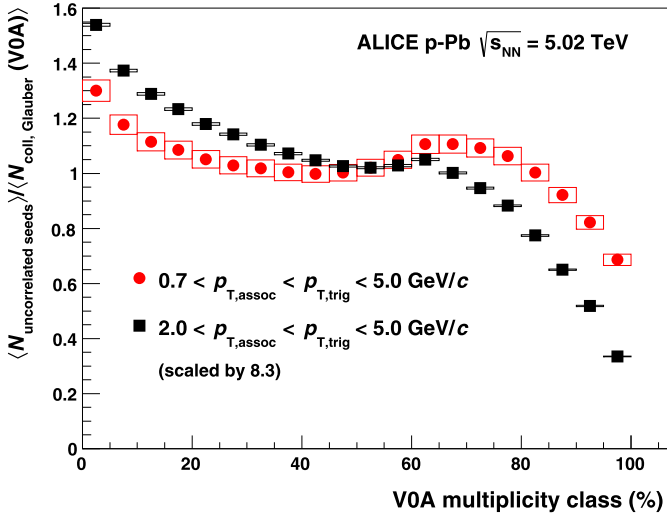


Fig. 6. Ratio between uncorrelated seeds and N_{coll} estimated within the Glauber model as a function of VOA multiplicity class. Statistical (lines) and systematic uncertainties (boxes) are shown, even though the statistical ones are smaller than the symbol size. To aid the comparison, the higher p_T range has been scaled by a factor 8.3 to agree with the lower p_T range in the 50–55% multiplicity class.

Fig. 5 presents the uncorrelated seeds as a function of the midrapidity charged-particle multiplicity for two p_T cuts. In the range $2 \text{ GeV}/c < p_{T,\text{assoc}} < p_{T,\text{trig}} < 5 \text{ GeV}/c$, the number of uncorrelated seeds increases with multiplicity from about 0 to about 3. The uncorrelated seeds exhibit a linear increase with midrapidity charged particle multiplicity N_{ch} in particular at high multiplicity. To quantify this behaviour, a linear fit is performed in the 0–50% multiplicity class and the ratio to the data is presented in the bottom panel.

The linear description of the data is valid for $N_{\text{ch}} > 20$ while deviations at lower multiplicity are observed. Deviations from linearity are not surprising as other observables, e.g. the mean $\langle p_T \rangle$ [26] and the R_{pA} [27], show a change in dynamics as a function of multiplicity. In this p_T range, the uncorrelated seeds are rather similar to the number of particles above a certain p_T threshold as the denominator of Eq. (3) is close to unity. On the contrary, in the range $0.7 \text{ GeV}/c < p_{T,\text{assoc}} < p_{T,\text{trig}} < 5.0 \text{ GeV}/c$ the denominator is far from unity. In this region, the number of uncorrelated seeds increases with multiplicity from about 2 to about 20. The linear description extends over a slightly wider range but a departure is also observed at low multiplicity.

It is interesting to relate the number of uncorrelated seeds to the number of nucleon–nucleon collisions, which in heavy-ion collisions is described successfully by Glauber models [28] ($N_{\text{coll, Glauber}}$). However, in p–Pb collisions, ongoing studies [27] (to be published in [29]) indicate that modifications to the Glauber Monte-Carlo simulations are needed for a correct estimation of the number of hard processes.

Fig. 6 presents the ratio between uncorrelated seeds and $N_{\text{coll, Glauber}}$ (calculated with a Glauber Monte-Carlo simulation) as a function of VOA multiplicity class for two p_T cuts. A scaling of the uncorrelated seeds with $N_{\text{coll, Glauber}}$ within 3% is observed between 25% and 55% multiplicity classes. At higher multiplicity, for the $0.7 \text{ GeV}/c < p_{T,\text{assoc}} < p_{T,\text{trig}} < 5.0 \text{ GeV}/c$ ($2.0 \text{ GeV}/c < p_{T,\text{assoc}} < p_{T,\text{trig}} < 5.0 \text{ GeV}/c$) range, the ratio between the number of uncorrelated seeds and the number of collisions estimated within the Glauber Monte-Carlo simulations deviates up to 25% (60%) from its average. At low multiplicity the deviation is about 30% (25%). This shows that contrary to the expectation for a semi-hard process, the number of uncorrelated seeds is not strictly proportional to the number of binary collisions. For further de-

tails, we refer the reader to the publication Ref. [29], which is in preparation. Some of these deviations could be due to a bias induced by the centrality estimator. Monte-Carlo simulations indicate that by using multiplicity to define event classes, a bias on the mean number of hard collisions per event is introduced: high (low) multiplicity bias towards events with higher (lower) number of semi-hard processes. In addition, low-multiplicity p–Pb events result from collisions with a larger than average proton–nucleus impact parameter, which, for peripheral collisions, corresponds also to a larger than average proton–nucleon impact parameter [30]. Therefore, in low-multiplicity collisions the number of MPIs is expected to decrease, which is consistent with the measurement.

6. Summary

Two-particle angular correlations of charged particles have been measured in p–Pb collisions at $\sqrt{s_{\text{NN}}} = 5.02 \text{ TeV}$ and expressed as associated yields per trigger particle. Long-range pseudorapidity correlations have been subtracted from the per-trigger yields in order to study the jet-like correlation peaks. Near-side and away-side jet-like yields are found to be approximately constant over a large range in multiplicity, with the exception of events with low multiplicity. This indicates that at high multiplicity hard processes and number of soft particles have the same evolution with multiplicity. These findings are consistent with a picture where independent parton–parton scatterings with subsequent incoherent fragmentation produce the measured minijet associated yields, while the ridge yields, which vary with multiplicity, are the result of other sources. This imposes significant constraints on models which aim at describing p–Pb collisions. They must reproduce such an incoherent superposition while also describing observations like the ridge structures and the increase of mean p_T with event multiplicity.

The number of uncorrelated seeds increases almost linearly with multiplicity, except at very low multiplicity. Thus, within the measured range, there is no evidence of a saturation in the number of multiple parton interactions. Furthermore, it is observed that the number of uncorrelated seeds scales only in the intermediate multiplicity region with the number of binary nucleon–nucleon collisions estimated with Glauber Monte-Carlo simulations, while at high and low multiplicities some biases could possibly cause the scale breaking.

Acknowledgements

The ALICE Collaboration would like to thank all its engineers and technicians for their invaluable contributions to the construction of the experiment and the CERN accelerator teams for the outstanding performance of the LHC complex. The ALICE Collaboration gratefully acknowledges the resources and support provided by all Grid centres and the Worldwide LHC Computing Grid (WLCG) collaboration. The ALICE Collaboration acknowledges the following funding agencies for their support in building and running the ALICE detector: State Committee of Science, World Federation of Scientists (WFS) and Swiss Fonds Kidagan, Armenia, Conselho Nacional de Desenvolvimento Científico e Tecnológico (CNPq), Financiadora de Estudos e Projetos (FINEP), Fundação de Amparo à Pesquisa do Estado de São Paulo (FAPESP); National Natural Science Foundation of China (NSFC), the Chinese Ministry of Education (CMOE) and the Ministry of Science and Technology of China (MSTC); Ministry of Education and Youth of the Czech Republic; Danish Natural Science Research Council, the Carlsberg Foundation and the Danish National Research Foundation; The European Research Council under the European Community’s Seventh Framework Programme; Helsinki Institute of Physics and the Academy

of Finland; French CNRS-IN2P3, the 'Region Pays de Loire', 'Region Alsace', 'Region Auvergne' and CEA, France; German BMBF and the Helmholtz Association; General Secretariat for Research and Technology, Ministry of Development, Greece; Hungarian OTKA and National Office for Research and Technology (NKTH); Department of Atomic Energy and Department of Science and Technology of the Government of India; Istituto Nazionale di Fisica Nucleare (INFN) and Centro Fermi – Museo Storico della Fisica e Centro Studi e Ricerche "Enrico Fermi", Italy; MEXT Grant-in-Aid for Specially Promoted Research, Japan; Joint Institute for Nuclear Research, Dubna; National Research Foundation of Korea (NRF); CONACYT, DGAPA, México, ALFA-EC and the EPLANET Program (European Particle Physics Latin American Network) Stichting voor Fundamenteel Onderzoek der Materie (FOM) and the Nederlandse Organisatie voor Wetenschappelijk Onderzoek (NWO), Netherlands; Research Council of Norway (NFR); Polish Ministry of Science and Higher Education; National Science Centre, Poland; Ministry of National Education/Institute for Atomic Physics and CNCS-UEFISCDI, Romania; Ministry of Education and Science of Russian Federation, Russian Academy of Sciences, Russian Federal Agency of Atomic Energy, Russian Federal Agency for Science and Innovations and The Russian Foundation for Basic Research; Ministry of Education of Slovakia; Department of Science and Technology, South Africa; CIEMAT, EELA, Ministerio de Economía y Competitividad (MINECO) of Spain, Xunta de Galicia (Consellería de Educación), CEADEN, Cubaenergía, Cuba, and IAEA (International Atomic Energy Agency); Swedish Research Council (VR) and Knut & Alice Wallenberg Foundation (KAW); Ukraine Ministry of Education and Science; United Kingdom Science and Technology Facilities Council (STFC); The United States Department of Energy, the United States National Science Foundation, the State of Texas, and the State of Ohio.

References

- [1] S. Chatrchyan, et al., Observation of long-range near-side angular correlations in proton–lead collisions at the LHC, *Phys. Lett. B* 718 (2013) 795–814.
- [2] B. Abelev, et al., Long-range angular correlations on the near and away side in p–Pb collisions at $\sqrt{s_{NN}} = 5.02$ TeV, *Phys. Lett. B* 719 (2013) 29–41.
- [3] G. Aad, et al., Measurement with the ATLAS detector of multi-particle azimuthal correlations in p+Pb collisions at $\sqrt{s_{NN}} = 5.02$ TeV, *Phys. Lett. B* 725 (2013) 60–78.
- [4] S. Chatrchyan, et al., Multiplicity and transverse momentum dependence of two- and four-particle correlations in pPb and PbPb collisions, *Phys. Lett. B* 724 (2013) 213–240.
- [5] G. Aad, et al., Measurement with the ATLAS detector of multi-particle azimuthal correlations in p–Pb collisions at $\sqrt{s_{NN}} = 5.02$ TeV, 2013.
- [6] B.B. Abelev, et al., Long-range angular correlations of pi, K and p in p–Pb collisions at $\sqrt{s_{NN}} = 5.02$ TeV, *Phys. Lett. B* 726 (2013) 164–177.

- [7] B. Abelev, et al., Anisotropic flow of charged hadrons, pions and (anti-)protons measured at high transverse momentum in Pb–Pb collisions at $\sqrt{s_{NN}} = 2.76$ TeV, *Phys. Lett. B* 719 (2013) 18–28.
- [8] P. Bozek, Collective flow in p–Pb and d–Pd collisions at TeV energies, *Phys. Rev. C* 85 (2012) 014911.
- [9] P. Bozek, W. Broniowski, Correlations from hydrodynamic flow in p–Pb collisions, *Phys. Lett. B* 718 (2013) 1557–1561.
- [10] P. Bozek, W. Broniowski, Collective dynamics in high-energy proton–nucleus collisions, *Phys. Rev. C* 88 (2013) 014903.
- [11] K. Werner, M. Bleicher, B. Guiot, I. Karpenko, T. Pierog, Evidence for flow in pPb collisions at 5 TeV from v2 mass splitting, 2013.
- [12] K. Werner, B. Guiot, I. Karpenko, T. Pierog, Analysing radial flow features in p–Pb and p–p collisions at several TeV by studying identified particle production in EPOS3, 2013.
- [13] K. Dusling, R. Venugopalan, Explanation of systematics of CMS p+Pb high multiplicity di-hadron data at $\sqrt{s_{NN}} = 5.02$ TeV, *Phys. Rev. D* 87 (2013) 054014.
- [14] K. Dusling, R. Venugopalan, Comparison of the color glass condensate to di-hadron correlations in proton–proton and proton–nucleus collisions, *Phys. Rev. D* 87 (2013) 094034.
- [15] B. Abelev, et al., Transverse momentum distribution and nuclear modification factor of charged particles in p–Pb collisions at $\sqrt{s_{NN}} = 5.02$ TeV, *Phys. Rev. Lett.* 110 (2013) 082302.
- [16] S. Chatrchyan, et al., Studies of dijet pseudorapidity distributions and transverse momentum balance in pPb collisions at $\sqrt{s_{NN}} = 5.02$ TeV, 2014.
- [17] I.M. Dremin, V.A. Nechitailo, Soft multiple parton interactions as seen in multiplicity distributions at tevatron and lhc, *Phys. Rev. D* 84 (2011) 034026.
- [18] J.F. Grosse-Oetringhaus, K. Reygers, Charged-particle multiplicity in proton–proton collisions, *J. Phys. G* 37 (2010) 083001.
- [19] B. Abelev, et al., Multiplicity dependence of two-particle azimuthal correlations in pp collisions at the LHC, *J. High Energy Phys.* 1309 (2013) 049.
- [20] K. Aamodt, et al., The ALICE experiment at the CERN LHC, *J. Instrum.* 3 (2008) S08002.
- [21] B. Abelev, et al., Pseudorapidity density of charged particles p–Pb collisions at $\sqrt{s_{NN}} = 5.02$ TeV, *Phys. Rev. Lett.* 110 (2013) 032301.
- [22] B. Abelev, et al., Centrality dependence of charged particle production at large transverse momentum in Pb–Pb collisions at $\sqrt{s_{NN}} = 2.76$ TeV, *Phys. Lett. B* 720 (2013) 52–62.
- [23] S. Roesler, R. Engel, J. Ranft, The Monte Carlo event generator DPMJET-III, 2000, pp. 1033–1038.
- [24] R. Brun, et al., GEANT detector description and simulation tool, CERN Program Library Long Write-up W5013 (1994).
- [25] X.-N. Wang, M. Gyulassy, HJING: a Monte Carlo model for multiple jet production in pp, pA and AA collisions, *Phys. Rev. D* 44 (1991) 3501.
- [26] B.B. Abelev, et al., Multiplicity dependence of the average transverse momentum in pp, p–Pb, and Pb–Pb collisions at the LHC, *Phys. Lett. B* 727 (2013) 371–380.
- [27] A. Morsch, p–Pb results from ALICE with an emphasis on centrality determination, *J. Phys. Conf. Ser.* 509 (2014) 012021.
- [28] M. Miller, K. Reygers, S. Sanders, P. Steinberg, Glauber modeling in high energy nuclear collisions, *Annu. Rev. Nucl. Part. Sci.* 57 (2007) 205–243.
- [29] B. Abelev, et al., Centrality dependence of particle production in p–Pb collisions at $\sqrt{s_{NN}} = 5.02$ TeV in the ALICE experiment, in preparation, 2014.
- [30] J. Jia, Influence of the nucleon–nucleon collision geometry on the determination of the nuclear modification factor for nucleon–nucleus and nucleus–nucleus collisions, *Phys. Lett. B* 681 (2009) 320–325.

ALICE Collaboration

B. Abelev^{bq}, J. Adam^{ak}, D. Adamová^{by}, M.M. Aggarwal^{cc}, M. Agnello^{da,cj}, A. Agostinelli^z, N. Agrawal^{ar}, Z. Ahammed^{dt}, N. Ahmad^r, I. Ahmed^o, S.U. Ahn^{bj}, S.A. Ahn^{bj}, I. Aimo^{da,cj}, S. Aiola^{dy}, M. Ajaz^o, A. Akindinov^{ba}, S.N. Alam^{dt}, D. Aleksandrov^{cp}, B. Alessandro^{da}, D. Alexandre^{cr}, A. Alici^{l,cu}, A. Alkin^c, J. Alme^{ai}, T. Alt^{am}, S. Altinpinar^q, I. Altsybeev^{ds}, C. Alves Garcia Prado^{di}, C. Andrei^{bt}, A. Andronic^{cm}, V. Anguelov^{ci}, J. Anielski^{aw}, T. Antičić^{cn}, F. Antinori^{cx}, P. Antonioli^{cu}, L. Aphecetche^{dc}, H. Appelshäuser^{av}, S. Arcelli^z, N. Armesto^p, R. Arnaldi^{da}, T. Aronsson^{dy}, I.C. Arsene^{cm}, M. Arslandok^{av}, A. Augustinus^{ah}, R. Averbeck^{cm}, T.C. Awes^{bz}, M.D. Azmi^{ce}, M. Bach^{am}, A. Badalà^{cw}, Y.W. Baek^{bl,an}, S. Bagnasco^{da}, R. Bailhache^{av}, R. Bala^{cf}, A. Baldisseriⁿ, F. Baltasar Dos Santos Pedrosa^{ah}, R.C. Baral^{bd}, R. Barbera^{aa}, F. Barile^{ae}, G.G. Barnaföldi^{dx}, L.S. Barnby^{cr}, V. Barret^{bl}, J. Bartke^{df}, M. Basile^z, N. Bastid^{bl}, S. Basu^{dt}, B. Bathen^{aw}, G. Batigne^{dc}, A. Batista Camejo^{bl}, B. Batyunya^{bi}, P.C. Batzing^u, C. Baumann^{av}, I.G. Bearden^{bv}, H. Beck^{av}, C. Bedda^{cj}, N.K. Behera^{ar}, I. Belikov^{ax}, F. Bellini^z, R. Bellwied^{dk}, E. Belmont-Moreno^{bg}, R. Belmont III^{dw}, V. Belyaev^{br}, G. Bencedi^{dx}, S. Beole^y, I. Berceanu^{bt},

A. Bercuci^{bt}, Y. Berdnikov^{ca,1}, D. Berenyi^{dx}, M.E. Berger^{ch}, R.A. Bertens^{az}, D. Berzano^y, L. Betev^{ah},
 A. Bhasin^{cf}, I.R. Bhat^{cf}, A.K. Bhati^{cc}, B. Bhattacharjee^{ao}, J. Bhom^{dp}, L. Bianchi^y, N. Bianchi^{bn},
 C. Bianchin^{az}, J. Bielčik^{ak}, J. Bielčíková^{by}, A. Bilandzic^{bv}, S. Bjelogrić^{az}, F. Blanco^j, D. Blau^{cp},
 C. Blume^{av}, F. Bock^{ci,bp}, A. Bogdanov^{br}, H. Bøggild^{bv}, M. Bogolyubsky^{db}, F.V. Böhmer^{ch}, L. Boldizsár^{dx},
 M. Bombara^{al}, J. Book^{av}, H. Borelⁿ, A. Borissov^{cl,dw}, F. Bossú^{bh}, M. Botje^{bw}, E. Botta^y, S. Böttger^{au},
 P. Braun-Munzinger^{cm}, M. Bregant^{di}, T. Breitner^{au}, T.A. Broker^{av}, T.A. Browning^{ck}, M. Broz^{ak},
 E. Bruna^{da}, G.E. Bruno^{ae}, D. Budnikov^{co}, H. Buesching^{av}, S. Bufalino^{da}, P. Buncic^{ah}, O. Busch^{ci},
 Z. Buthelezi^{bh}, D. Caffarri^{ab}, X. Cai^g, H. Caines^{dy}, L. Calero Diaz^{bn}, A. Caliva^{az}, E. Calvo Villar^{cs},
 P. Camerini^x, F. Carena^{ah}, W. Carena^{ah}, J. Castillo Castellanosⁿ, E.A.R. Casula^w, V. Catanescu^{bt},
 C. Cavicchioli^{ah}, C. Ceballos Sanchezⁱ, J. Cepila^{ak}, P. Cerello^{da}, B. Chang^{dl}, S. Chapeland^{ah}, J.L. Charvetⁿ,
 S. Chattopadhyay^{dt}, S. Chattopadhyay^{cq}, V. Chelnokov^c, M. Cherney^{cb}, C. Cheshkov^{dr}, B. Cheynis^{dr},
 V. Chibante Barroso^{ah}, D.D. Chinellato^{dk}, P. Chochula^{ah}, M. Chojnacki^{bv}, S. Choudhury^{dt},
 P. Christakoglou^{bw}, C.H. Christensen^{bv}, P. Christiansen^{af}, T. Chujo^{dp}, S.U. Chung^{cl}, C. Cicalo^{cv},
 L. Cifarelli^{z,l}, F. Cindolo^{cu}, J. Cleymans^{ce}, F. Colamaria^{ae}, D. Colella^{ae}, A. Collu^w, M. Colocci^z,
 G. Conesa Balbastre^{bm}, Z. Conesa del Valle^{at}, M.E. Connors^{dy}, J.G. Contreras^k, T.M. Cormier^{dw},
 Y. Corrales Morales^y, P. Cortese^{ad}, I. Cortés Maldonado^b, M.R. Cosentino^{di}, F. Costa^{ah}, P. Crochet^{bl},
 R. Cruz Albino^k, E. Cuautle^{bf}, L. Cunqueiro^{bn}, A. Dainese^{cx}, R. Dang^g, A. Danu^{be}, D. Das^{cq}, I. Das^{at},
 K. Das^{cq}, S. Das^d, A. Dash^{dj}, S. Dash^{ar}, S. De^{dt}, H. Delagrangé^{dc,2}, A. Deloff^{bs}, E. Dénes^{dx},
 G. D’Erasmus^{ae}, A. De Caro^{ac,l}, G. de Cataldo^{ct}, J. de Cuveland^{am}, A. De Falco^w, D. De Gruttola^{ac,l},
 N. De Marco^{da}, S. De Pasquale^{ac}, R. de Rooij^{az}, M.A. Diaz Corchero^j, T. Dietel^{aw}, P. Dillenseger^{av},
 R. Divià^{ah}, D. Di Bari^{ae}, S. Di Liberto^{cy}, A. Di Mauro^{ah}, P. Di Nezza^{bn}, Ø. Djuvsland^q, A. Dobrin^{az},
 T. Dobrowolski^{bs}, D. Domenicis Gimenez^{di}, B. Dönigus^{av}, O. Dordic^u, S. Dørheim^{ch}, A.K. Dubey^{dt},
 A. Dubla^{az}, L. Ducroux^{dr}, P. Dupieux^{bl}, A.K. Dutta Majumdar^{cq}, T.E. Hilden^{ap}, R.J. Ehlers^{dy}, D. Elia^{ct},
 H. Engel^{au}, B. Erazmus^{ah,dc}, H.A. Erdal^{ai}, D. Eschweiler^{am}, B. Espagnon^{at}, M. Esposito^{ah}, M. Estienne^{dc},
 S. Esumi^{dp}, D. Evans^{cr}, S. Evdokimov^{db}, D. Fabris^{cx}, J. Faivre^{bm}, D. Falchieri^z, A. Fantoni^{bn}, M. Fasel^{ci},
 D. Fehlfker^q, L. Feldkamp^{aw}, D. Felea^{be}, A. Feliciello^{da}, G. Feofilov^{ds}, J. Ferencei^{by}, A. Fernández Téllez^b,
 E.G. Ferreira^p, A. Ferretti^y, A. Festanti^{ab}, J. Figiel^{df}, M.A.S. Figueredo^{dm}, S. Filchagin^{co}, D. Finogeev^{ay},
 F.M. Fionda^{ae}, E.M. Fiore^{ae}, E. Floratos^{cd}, M. Floris^{ah}, S. Foertsch^{bh}, P. Foka^{cm}, S. Fokin^{cp},
 E. Fragiaco^{cz}, A. Francescon^{ah,ab}, U. Frankenfeld^{cm}, U. Fuchs^{ah}, C. Furget^{bm}, M. Fusco Girard^{ac},
 J.J. Gaardhøje^{bv}, M. Gagliardi^y, A.M. Gago^{cs}, M. Gallio^y, D.R. Gangadharan^s, P. Ganoti^{bz}, C. Garabatos^{cm},
 E. Garcia-Solis^m, C. Gargiulo^{ah}, I. Garishvili^{bq}, J. Gerhard^{am}, M. Germain^{dc}, A. Gheata^{ah}, M. Gheata^{ah,be},
 B. Ghidini^{ae}, P. Ghosh^{dt}, S.K. Ghosh^d, P. Gianotti^{bn}, P. Giubellino^{ah}, E. Gladysz-Dziadus^{df}, P. Glässel^{ci},
 A. Gomez Ramirez^{au}, P. González-Zamora^j, S. Gorbunov^{am}, L. Görlich^{df}, S. Gotovac^{de},
 L.K. Graczykowski^{dv}, A. Grelli^{az}, A. Grigoras^{ah}, C. Grigoras^{ah}, V. Grigoriev^{br}, A. Grigoryan^a,
 S. Grigoryan^{bi}, B. Grinyov^c, N. Grion^{cz}, J.F. Grosse-Oetringhaus^{ah}, J.-Y. Grossiord^{dr}, R. Grosso^{ah},
 F. Guber^{ay}, R. Guernane^{bm}, B. Guerzoni^z, M. Guilbaud^{dr}, K. Gulbrandsen^{bv}, H. Gulkanyan^a,
 M. Gumbo^{ce}, T. Gunji^{do}, A. Gupta^{cf}, R. Gupta^{cf}, K.H. Khan^o, R. Haake^{aw}, Ø. Haaland^q, C. Hadjidakis^{at},
 M. Haiduc^{be}, H. Hamagaki^{do}, G. Hamar^{dx}, L.D. Hanratty^{cr}, A. Hansen^{bv}, J.W. Harris^{dy}, H. Hartmann^{am},
 A. Harton^m, D. Hatzifotiadou^{cu}, S. Hayashi^{do}, S.T. Heckel^{av}, M. Heide^{aw}, H. Helstrup^{ai}, A. Herghelegiu^{bt},
 G. Herrera Corral^k, B.A. Hess^{ag}, K.F. Hetland^{ai}, B. Hippolyte^{ax}, J. Hladky^{bc}, P. Hristov^{ah}, M. Huang^q,
 T.J. Humanic^s, N. Hussain^{ao}, D. Hutter^{am}, D.S. Hwang^t, R. Ilkaev^{co}, I. Ilkiv^{bs}, M. Inaba^{dp},
 G.M. Innocenti^y, C. Ionita^{ah}, M. Ippolitov^{cp}, M. Irfan^r, M. Ivanov^{cm}, V. Ivanov^{ca}, A. Jachołkowski^{aa},
 P.M. Jacobs^{bp}, C. Jahnke^{di}, H.J. Jang^{bj}, M.A. Janik^{dv}, P.H.S.Y. Jayarathna^{dk}, C. Jena^{ab}, S. Jena^{dk},
 R.T. Jimenez Bustamante^{bf}, P.G. Jones^{cr}, H. Jung^{an}, A. Jusko^{cr}, V. Kadyshevskiy^{bi}, S. Kalcher^{am},
 P. Kalinak^{bb}, A. Kalweit^{ah}, J. Kamin^{av}, J.H. Kang^{dz}, V. Kaplin^{br}, S. Kar^{dt}, A. Karasu Uysal^{bk},
 O. Karavichev^{ay}, T. Karavicheva^{ay}, E. Karpechev^{ay}, U. Keschull^{au}, R. Keidel^{ea}, D.L.D. Keijdener^{az},
 M.M. Khan^{r,3}, P. Khan^{cq}, S.A. Khan^{dt}, A. Khanzadeev^{ca}, Y. Kharlov^{db}, B. Kileng^{ai}, B. Kim^{dz},
 D.W. Kim^{bj,an}, D.J. Kim^{dl}, J.S. Kim^{an}, M. Kim^{an}, M. Kim^{dz}, S. Kim^t, T. Kim^{dz}, S. Kirsch^{am}, I. Kisel^{am},
 S. Kiselev^{ba}, A. Kisiel^{dv}, G. Kiss^{dx}, J.L. Klay^f, J. Klein^{ci}, C. Klein-Bösing^{aw}, A. Kluge^{ah}, M.L. Knichel^{cm},
 A.G. Knospe^{dg}, C. Kobdaj^{ah,dd}, M. Kofarago^{ah}, M.K. Köhler^{cm}, T. Kollegger^{am}, A. Kolojvari^{ds},
 V. Kondratiev^{ds}, N. Kondratyeva^{br}, A. Konevskikh^{ay}, V. Kovalenko^{ds}, M. Kowalski^{df}, S. Kox^{bm},
 G. Koyithatta Meethalevedu^{ar}, J. Kral^{dl}, I. Králik^{bb}, F. Kramer^{av}, A. Kravčáková^{al}, M. Krelina^{ak},

M. Kretz ^{am}, M. Krivda ^{cr,bb}, F. Krizek ^{by}, E. Kryshen ^{ah}, M. Krzewicki ^{cm}, V. Kučera ^{by}, Y. Kucheriaev ^{cp,2}, T. Kugathasan ^{ah}, C. Kuhn ^{ax}, P.G. Kuijter ^{bw}, I. Kulakov ^{av}, J. Kumar ^{ar}, P. Kurashvili ^{bs}, A. Kurepin ^{ay}, A.B. Kurepin ^{ay}, A. Kuryakin ^{co}, S. Kushpil ^{by}, M.J. Kweon ^{ci}, Y. Kwon ^{dz}, P. Ladron de Guevara ^{bf}, C. Lagana Fernandes ^{di}, I. Lakomov ^{at}, R. Langoy ^{du}, C. Lara ^{au}, A. Lardeux ^{dc}, A. Lattuca ^y, S.L. La Pointe ^{az}, P. La Rocca ^{aa}, R. Lea ^x, L. Leardini ^{ci}, G.R. Lee ^{cr}, I. Legrand ^{ah}, J. Lehnert ^{av}, R.C. Lemmon ^{bx}, V. Lenti ^{ct}, E. Leogrande ^{az}, M. Leoncino ^y, I. León Monzón ^{dh}, P. Lévai ^{dx}, S. Li ^{bl,g}, J. Lien ^{du}, R. Lietava ^{cr}, S. Lindal ^u, V. Lindenstruth ^{am}, C. Lippmann ^{cm}, M.A. Lisa ^s, H.M. Ljunggren ^{af}, D.F. Lodato ^{az}, P.I. Loenne ^q, V.R. Loggins ^{dw}, V. Loginov ^{br}, D. Lohner ^{ci}, C. Loizides ^{bp}, X. Lopez ^{bl}, E. López Torres ⁱ, X.-G. Lu ^{ci}, P. Luettig ^{av}, M. Lunardon ^{ab}, G. Luparello ^{az}, R. Ma ^{dy}, A. Maevskaya ^{ay}, M. Mager ^{ah}, D.P. Mahapatra ^{bd}, S.M. Mahmood ^u, A. Maire ^{ci}, R.D. Majka ^{dy}, M. Malaev ^{ca}, I. Maldonado Cervantes ^{bf}, L. Malinina ^{bi,4}, D. Mal'Kevich ^{ba}, P. Malzacher ^{cm}, A. Mamonov ^{co}, L. Manceau ^{da}, V. Manko ^{cp}, F. Manso ^{bl}, V. Manzari ^{ct}, M. Marchisone ^{bl,y}, J. Mareš ^{bc}, G.V. Margagliotti ^x, A. Margotti ^{cu}, A. Marín ^{cm}, C. Markert ^{dg}, M. Marquard ^{av}, I. Martashvili ^{dn}, N.A. Martin ^{cm}, P. Martinengo ^{ah}, M.I. Martínez ^b, G. Martínez García ^{dc}, J. Martin Blanco ^{dc}, Y. Martynov ^c, A. Mas ^{dc}, S. Masciocchi ^{cm}, M. Maserà ^y, A. Masoni ^{cv}, L. Massacrier ^{dc}, A. Mastroserio ^{ae}, A. Matyja ^{df}, C. Mayer ^{df}, J. Mazer ^{dn}, M.A. Mazzoni ^{cy}, F. Meddi ^v, A. Menchaca-Rocha ^{bg}, J. Mercado Pérez ^{ci}, M. Meres ^{aj}, Y. Miake ^{dp}, K. Mikhaylov ^{bi,ba}, L. Milano ^{ah}, J. Milosevic ^{u,1,5}, A. Mischke ^{az}, A.N. Mishra ^{as}, D. Miśkowiec ^{cm}, J. Mitra ^{dt}, C.M. Mitu ^{be}, J. Mlynarz ^{dw}, N. Mohammadi ^{az}, B. Mohanty ^{bu,dt}, L. Molnar ^{ax}, L. Montaño Zetina ^k, E. Montes ^j, M. Morando ^{ab}, D.A. Moreira De Godoy ^{di}, S. Moretto ^{ab}, A. Morsch ^{ah}, V. Muccifora ^{bn}, E. Mudnic ^{de}, D. Mühlheim ^{aw}, S. Muhuri ^{dt}, M. Mukherjee ^{dt}, H. Müller ^{ah}, M.G. Munhoz ^{di}, S. Murray ^{ce}, L. Musa ^{ah}, J. Musinsky ^{bb}, B.K. Nandi ^{ar}, R. Nania ^{cu}, E. Nappi ^{ct}, C. Nattrass ^{dn}, K. Nayak ^{bu}, T.K. Nayak ^{dt}, S. Nazarenko ^{co}, A. Nedosekin ^{ba}, M. Nicassio ^{cm}, M. Niculescu ^{ah,be}, B.S. Nielsen ^{bv}, S. Nikolaev ^{cp}, S. Nikulin ^{cp}, V. Nikulin ^{ca}, B.S. Nilsen ^{cb}, F. Noferini ^{l,cu}, P. Nomokonov ^{bi}, G. Nooren ^{az}, J. Norman ^{dm}, A. Nyanin ^{cp}, J. Nystrand ^q, H. Oeschler ^{ci}, S. Oh ^{dy}, S.K. Oh ^{an,1,6}, A. Okatan ^{bk}, L. Olah ^{dx}, J. Oleniacz ^{dv}, A.C. Oliveira Da Silva ^{di}, J. Onderwaater ^{cm}, C. Oppedisano ^{da}, A. Ortiz Velasquez ^{af}, A. Oskarsson ^{af}, J. Otwinowski ^{cm}, K. Oyama ^{ci}, P. Sahoo ^{as}, Y. Pachmayer ^{ci}, M. Pachr ^{ak}, P. Pagano ^{ac}, G. Paic ^{bf}, F. Painke ^{am}, C. Pajares ^p, S.K. Pal ^{dt}, A. Palmeri ^{cw}, D. Pant ^{ar}, V. Papikyan ^a, G.S. Pappalardo ^{cw}, P. Pareek ^{as}, W.J. Park ^{cm}, S. Parmar ^{cc}, A. Passfeld ^{aw}, D.I. Patalakha ^{db}, V. Paticchio ^{ct}, B. Paul ^{cq}, T. Pawlak ^{dv}, T. Peitzmann ^{az}, H. Pereira Da Costa ⁿ, E. Pereira De Oliveira Filho ^{di}, D. Peresunko ^{cp}, C.E. Pérez Lara ^{bw}, A. Pesci ^{cu}, V. Peskov ^{av}, Y. Pestov ^e, V. Petráček ^{ak}, M. Petran ^{ak}, M. Petris ^{bt}, M. Petrovici ^{bt}, C. Petta ^{aa}, S. Piano ^{cz}, M. Pikna ^{aj}, P. Pillot ^{dc}, O. Pinazza ^{cu,ah}, L. Pinsky ^{dk}, D.B. Piyarathna ^{dk}, M. Płoskoń ^{bp}, M. Planinic ^{dq,cn}, J. Pluta ^{dv}, S. Pochybova ^{dx}, P.L.M. Podesta-Lerma ^{dh}, M.G. Poghosyan ^{ah}, E.H.O. Pohjoisaho ^{ap}, B. Polichtchouk ^{db}, N. Poljak ^{cn}, A. Pop ^{bt}, S. Porteboeuf-Houssais ^{bl}, J. Porter ^{bp}, B. Potukuchi ^{cf}, S.K. Prasad ^{dw}, R. Preghenella ^{cu,l}, F. Prino ^{da}, C.A. Pruneau ^{dw}, I. Pshenichnov ^{ay}, G. Puddu ^w, P. Pujahari ^{dw}, V. Punin ^{co}, J. Putschke ^{dw}, H. Qvigstad ^u, A. Rachevski ^{cz}, S. Raha ^d, J. Rak ^{dl}, A. Rakotozafindrabe ⁿ, L. Ramello ^{ad}, R. Raniwala ^{cg}, S. Raniwala ^{cg}, S.S. Räsänen ^{ap}, B.T. Rascanu ^{av}, D. Rathee ^{cc}, A.W. Rauf ^o, V. Razazi ^w, K.F. Read ^{dn}, J.S. Real ^{bm}, K. Redlich ^{bs,1,7}, R.J. Reed ^{dy}, A. Rehman ^q, P. Reichelt ^{av}, M. Reicher ^{az}, F. Reidt ^{ah}, R. Renfordt ^{av}, A.R. Reolon ^{bn}, A. Reshetin ^{ay}, F. Rettig ^{am}, J.-P. Revol ^{ah}, K. Reygers ^{ci}, V. Riabov ^{ca}, R.A. Ricci ^{bo}, T. Richert ^{af}, M. Richter ^u, P. Riedler ^{ah}, W. Riegler ^{ah}, F. Riggi ^{aa}, A. Rivetti ^{da}, E. Rocco ^{az}, M. Rodríguez Cahuantzi ^b, A. Rodríguez Manso ^{bw}, K. Røed ^u, E. Rogochaya ^{bi}, S. Rohni ^{cf}, D. Rohr ^{am}, D. Röhrich ^q, R. Romita ^{bx}, F. Ronchetti ^{bn}, L. Ronflette ^{dc}, P. Rosnet ^{bl}, A. Rossi ^{ah}, F. Roukoutakis ^{cd}, A. Roy ^{as}, C. Roy ^{ax}, P. Roy ^{cq}, A.J. Rubio Montero ^j, R. Rui ^x, R. Russo ^y, E. Ryabinkin ^{cp}, Y. Ryabov ^{ca}, A. Rybicki ^{df}, S. Sadovsky ^{db}, K. Šafařík ^{ah}, B. Sahlmüller ^{av}, R. Sahoo ^{as}, P.K. Sahu ^{bd}, J. Saini ^{dt}, S. Sakai ^{bp}, C.A. Salgado ^p, J. Salzwedel ^s, S. Sambyal ^{cf}, V. Samsonov ^{ca}, X. Sanchez Castro ^{ax}, F.J. Sánchez Rodríguez ^{dh}, L. Šándor ^{bb}, A. Sandoval ^{bg}, M. Sano ^{dp}, G. Santagati ^{aa}, D. Sarkar ^{dt}, E. Scapparone ^{cu}, F. Scarlassara ^{ab}, R.P. Scharenberg ^{ck}, C. Schiava ^{bt}, R. Schicker ^{ci}, C. Schmidt ^{cm}, H.R. Schmidt ^{ag}, S. Schuchmann ^{av}, J. Schukraft ^{ah}, M. Schulc ^{ak}, T. Schuster ^{dy}, Y. Schutz ^{dc,ah}, K. Schwarz ^{cm}, K. Schweda ^{cm}, G. Scioli ^z, E. Scapparone ^{da}, R. Scott ^{dn}, G. Segato ^{ab}, J.E. Seger ^{cb}, Y. Sekiguchi ^{do}, I. Selyuzhenkov ^{cm}, J. Seo ^{cl}, E. Serradilla ^{j,bg}, A. Sevcenco ^{be}, A. Shabetai ^{dc}, G. Shabratova ^{bi}, R. Shahoyan ^{ah}, A. Shangaraev ^{db}, N. Sharma ^{dn}, S. Sharma ^{cf}, K. Shigaki ^{aq}, K. Shtejer ^y, Y. Sibiriak ^{cp}, E. Sicking ^{aw,ah}, S. Siddhanta ^{cv}, T. Siemiarczuk ^{bs}, D. Silvermyr ^{bz}, C. Silvestre ^{bm}, G. Simatovic ^{dq}, R. Singaraju ^{dt}, R. Singh ^{cf}, S. Singha ^{dt,bu}, V. Singhal ^{dt}, B.C. Sinha ^{dt}, T. Sinha ^{cq}, B. Sitar ^{aj}, M. Sitta ^{ad}, T.B. Skaali ^u, K. Skjerdal ^q, M. Slupecki ^{dl}, N. Smirnov ^{dy}, R.J.M. Snellings ^{az}, C. Søgaard ^{af},

R. Soltz^{bq}, J. Song^{cl}, M. Song^{dz}, F. Soramel^{ab}, S. Sorensen^{dn}, M. Spacek^{ak}, E. Spiriti^{bn}, I. Sputowska^{df}, M. Spyropoulou-Stassinaki^{cd}, B.K. Srivastava^{ck}, J. Stachel^{ci}, I. Stan^{be}, G. Stefanek^{bs}, M. Steinpreis^s, E. Stenlund^{af}, G. Steyn^{bh}, J.H. Stiller^{ci}, D. Stocco^{dc}, M. Stolpovskiy^{db}, P. Strmen^{aj}, A.A.P. Suaide^{di}, T. Sugitate^{aq}, C. Suire^{at}, M. Suleymanov^o, R. Sultanov^{ba}, M. Šumbera^{by}, T. Susa^{cn}, T.J.M. Symons^{bp}, A. Szabo^{aj}, A. Szanto de Toledo^{di}, I. Szarka^{aj}, A. Szczepankiewicz^{ah}, M. Szymanski^{dv}, J. Takahashi^{dj}, M.A. Tangaro^{ae}, J.D. Tapia Takaki^{at,1,8}, A. Tarantola Pelsoni^{av}, A. Tarazona Martinez^{ah}, M.G. Tarzila^{bt}, A. Tauro^{ah}, G. Tejada Muñoz^b, A. Telesca^{ah}, C. Terrevoli^w, J. Thäder^{cm}, D. Thomas^{az}, R. Tieulent^{dr}, A.R. Timmins^{dk}, A. Toia^{cx}, V. Trubnikov^c, W.H. Trzaska^{dl}, T. Tsuji^{do}, A. Tumkin^{co}, R. Turrisi^{cx}, T.S. Tveter^u, K. Ullaland^q, A. Uras^{dr}, G.L. Usai^w, M. Vajzer^{by}, M. Vala^{bb,bi}, L. Valencia Palomo^{bl}, S. Vallero^{ci}, P. Vande Vyvre^{ah}, J. Van Der Maarel^{az}, J.W. Van Hoorne^{ah}, M. van Leeuwen^{az}, A. Vargas^b, M. Vargyas^{dl}, R. Varma^{ar}, M. Vasileiou^{cd}, A. Vasiliev^{cp}, V. Vechernin^{ds}, M. Veldhoen^{az}, A. Velure^q, M. Venaruzzo^{x,bo}, E. Vercellin^y, S. Vergara Limón^b, R. Vernet^h, M. Verweij^{dw}, L. Vickovic^{de}, G. Viesti^{ab}, J. Viinikainen^{dl}, Z. Vilakazi^{bh}, O. Villalobos Baillie^{cr}, A. Vinogradov^{cp}, L. Vinogradov^{ds}, Y. Vinogradov^{co}, T. Virgili^{ac}, Y.P. Viyogi^{dt}, A. Vodopyanov^{bi}, M.A. Völkl^{ci}, K. Voloshin^{ba}, S.A. Voloshin^{dw}, G. Volpe^{ah}, B. von Haller^{ah}, I. Vorobyev^{ds}, D. Vranic^{ah,cm}, J. Vrláková^{al}, B. Vulpescu^{bl}, A. Vyushin^{co}, B. Wagner^q, J. Wagner^{cm}, V. Wagner^{ak}, M. Wang^{g,dc}, Y. Wang^{ci}, D. Watanabe^{dp}, M. Weber^{dk}, J.P. Wessels^{aw}, U. Westerhoff^{aw}, J. Wiechula^{ag}, J. Wikne^u, M. Wilde^{aw}, G. Wilk^{bs}, J. Wilkinson^{ci}, M.C.S. Williams^{cu}, B. Windelband^{ci}, M. Winn^{ci}, C.G. Yaldo^{dw}, Y. Yamaguchi^{do}, H. Yang^{az}, P. Yang^g, S. Yang^q, S. Yano^{aq}, S. Yasnopolskiy^{cp}, J. Yi^{cl}, Z. Yin^g, I.-K. Yoo^{cl}, I. Yushmanov^{cp}, V. Zaccaro^{bv}, C. Zach^{ak}, A. Zaman^o, C. Zampolli^{cu}, S. Zaporozhets^{bi}, A. Zarochentsev^{ds}, P. Závada^{bc}, N. Zaviyalov^{co}, H. Zbroszczyk^{dv}, I.S. Zgura^{be}, M. Zhalov^{ca}, H. Zhang^g, X. Zhang^{g,bp}, Y. Zhang^g, C. Zhao^u, N. Zhigareva^{ba}, D. Zhou^g, F. Zhou^g, Y. Zhou^{az}, Zhuo Zhou^q, H. Zhu^g, J. Zhu^g, X. Zhu^g, A. Zichichi^{l,z}, A. Zimmermann^{ci}, M.B. Zimmermann^{aw,ah}, G. Zinovjev^c, Y. Zoccarato^{dr}, M. Zyzak^{av}

^a A.I. Alikhanyan National Science Laboratory (Yerevan Physics Institute) Foundation, Yerevan, Armenia

^b Benemérita Universidad Autónoma de Puebla, Puebla, Mexico

^c Bogolyubov Institute for Theoretical Physics, Kiev, Ukraine

^d Bose Institute, Department of Physics and Centre for Astroparticle Physics and Space Science (CAPSS), Kolkata, India

^e Budker Institute for Nuclear Physics, Novosibirsk, Russia

^f California Polytechnic State University, San Luis Obispo, CA, United States

^g Central China Normal University, Wuhan, China

^h Centre de Calcul de l'IN2P3, Villeurbanne, France

ⁱ Centro de Aplicaciones Tecnológicas y Desarrollo Nuclear (CEADEN), Havana, Cuba

^j Centro de Investigaciones Energéticas Medioambientales y Tecnológicas (CIEMAT), Madrid, Spain

^k Centro de Investigación y de Estudios Avanzados (CINVESTAV), Mexico City and Mérida, Mexico

^l Centro Fermi – Museo Storico della Fisica e Centro Studi e Ricerche “Enrico Fermi”, Rome, Italy

^m Chicago State University, Chicago, USA

ⁿ Commissariat à l’Energie Atomique, IRFU, Saclay, France

^o COMSATS Institute of Information Technology (CIIT), Islamabad, Pakistan

^p Departamento de Física de Partículas and IGFAE, Universidad de Santiago de Compostela, Santiago de Compostela, Spain

^q Department of Physics and Technology, University of Bergen, Bergen, Norway

^r Department of Physics, Aligarh Muslim University, Aligarh, India

^s Department of Physics, Ohio State University, Columbus, OH, United States

^t Department of Physics, Sejong University, Seoul, South Korea

^u Department of Physics, University of Oslo, Oslo, Norway

^v Dipartimento di Fisica dell’Università ‘La Sapienza’ and Sezione INFN Rome, Italy

^w Dipartimento di Fisica dell’Università and Sezione INFN, Cagliari, Italy

^x Dipartimento di Fisica dell’Università and Sezione INFN, Trieste, Italy

^y Dipartimento di Fisica dell’Università and Sezione INFN, Turin, Italy

^z Dipartimento di Fisica e Astronomia dell’Università and Sezione INFN, Bologna, Italy

^{aa} Dipartimento di Fisica e Astronomia dell’Università and Sezione INFN, Catania, Italy

^{ab} Dipartimento di Fisica e Astronomia dell’Università and Sezione INFN, Padova, Italy

^{ac} Dipartimento di Fisica ‘E.R. Caianiello’ dell’Università and Gruppo Collegato INFN, Salerno, Italy

^{ad} Dipartimento di Scienze e Innovazione Tecnologica dell’Università del Piemonte Orientale and Gruppo Collegato INFN, Alessandria, Italy

^{ae} Dipartimento Interateneo di Fisica ‘M. Merlin’ and Sezione INFN, Bari, Italy

^{af} Division of Experimental High Energy Physics, University of Lund, Lund, Sweden

^{ag} Eberhard Karls Universität Tübingen, Tübingen, Germany

^{ah} European Organization for Nuclear Research (CERN), Geneva, Switzerland

^{ai} Faculty of Engineering, Bergen University College, Bergen, Norway

^{aj} Faculty of Mathematics, Physics and Informatics, Comenius University, Bratislava, Slovakia

^{ak} Faculty of Nuclear Sciences and Physical Engineering, Czech Technical University in Prague, Prague, Czech Republic

^{al} Faculty of Science, P.J. Šafárik University, Košice, Slovakia

^{am} Frankfurt Institute for Advanced Studies, Johann Wolfgang Goethe-Universität Frankfurt, Frankfurt, Germany

^{an} Gangneung-Wonju National University, Gangneung, South Korea

^{ao} Gauhati University, Department of Physics, Guwahati, India

^{ap} Helsinki Institute of Physics (HIP), Helsinki, Finland

^{aq} Hiroshima University, Hiroshima, Japan

- ^{ar} Indian Institute of Technology Bombay (IIT), Mumbai, India
- ^{as} Indian Institute of Technology Indore, Indore (IITI), India
- ^{at} Institut de Physique Nucléaire d'Orsay (IPNO), Université Paris-Sud, CNRS-IN2P3, Orsay, France
- ^{au} Institut für Informatik, Johann Wolfgang Goethe-Universität Frankfurt, Frankfurt, Germany
- ^{av} Institut für Kernphysik, Johann Wolfgang Goethe-Universität Frankfurt, Frankfurt, Germany
- ^{aw} Institut für Kernphysik, Westfälische Wilhelms-Universität Münster, Münster, Germany
- ^{ax} Institut Pluridisciplinaire Hubert Curien (IPHC), Université de Strasbourg, CNRS-IN2P3, Strasbourg, France
- ^{ay} Institute for Nuclear Research, Academy of Sciences, Moscow, Russia
- ^{az} Institute for Subatomic Physics of Utrecht University, Utrecht, Netherlands
- ^{ba} Institute for Theoretical and Experimental Physics, Moscow, Russia
- ^{bb} Institute of Experimental Physics, Slovak Academy of Sciences, Košice, Slovakia
- ^{bc} Institute of Physics, Academy of Sciences of the Czech Republic, Prague, Czech Republic
- ^{bd} Institute of Physics, Bhubaneswar, India
- ^{be} Institute of Space Science (ISS), Bucharest, Romania
- ^{bf} Instituto de Ciencias Nucleares, Universidad Nacional Autónoma de México, Mexico City, Mexico
- ^{bg} Instituto de Física, Universidad Nacional Autónoma de México, Mexico City, Mexico
- ^{bh} iThemba LABS, National Research Foundation, Somerset West, South Africa
- ^{bi} Joint Institute for Nuclear Research (JINR), Dubna, Russia
- ^{bj} Korea Institute of Science and Technology Information, Daejeon, South Korea
- ^{bk} KTO Karatay University, Konya, Turkey
- ^{bl} Laboratoire de Physique Corpusculaire (LPC), Clermont Université, Université Blaise Pascal, CNRS-IN2P3, Clermont-Ferrand, France
- ^{bm} Laboratoire de Physique Subatomique et de Cosmologie, Université Grenoble-Alpes, CNRS-IN2P3, Grenoble, France
- ^{bn} Laboratori Nazionali di Frascati, INFN, Frascati, Italy
- ^{bo} Laboratori Nazionali di Legnaro, INFN, Legnaro, Italy
- ^{bp} Lawrence Berkeley National Laboratory, Berkeley, CA, United States
- ^{bq} Lawrence Livermore National Laboratory, Livermore, CA, United States
- ^{br} Moscow Engineering Physics Institute, Moscow, Russia
- ^{bs} National Centre for Nuclear Studies, Warsaw, Poland
- ^{bt} National Institute for Physics and Nuclear Engineering, Bucharest, Romania
- ^{bu} National Institute of Science Education and Research, Bhubaneswar, India
- ^{bv} Niels Bohr Institute, University of Copenhagen, Copenhagen, Denmark
- ^{bw} Nikhef, National Institute for Subatomic Physics, Amsterdam, Netherlands
- ^{bx} Nuclear Physics Group, STFC Daresbury Laboratory, Daresbury, United Kingdom
- ^{by} Nuclear Physics Institute, Academy of Sciences of the Czech Republic, Řež u Prahy, Czech Republic
- ^{bz} Oak Ridge National Laboratory, Oak Ridge, TN, United States
- ^{ca} Petersburg Nuclear Physics Institute, Gatchina, Russia
- ^{cb} Physics Department, Creighton University, Omaha, NE, United States
- ^{cc} Physics Department, Panjab University, Chandigarh, India
- ^{cd} Physics Department, University of Athens, Athens, Greece
- ^{ce} Physics Department, University of Cape Town, Cape Town, South Africa
- ^{cf} Physics Department, University of Jammu, Jammu, India
- ^{cg} Physics Department, University of Rajasthan, Jaipur, India
- ^{ch} Physik Department, Technische Universität München, Munich, Germany
- ^{ci} Physikalisches Institut, Ruprecht-Karls-Universität Heidelberg, Heidelberg, Germany
- ^{cj} Politecnico di Torino, Turin, Italy
- ^{ck} Purdue University, West Lafayette, IN, United States
- ^{cl} Pusan National University, Pusan, South Korea
- ^{cm} Research Division and ExtreMe Matter Institute EMMI, GSI Helmholtzzentrum für Schwerionenforschung, Darmstadt, Germany
- ^{cn} Rudjer Bošković Institute, Zagreb, Croatia
- ^{co} Russian Federal Nuclear Center (VNIIEF), Sarov, Russia
- ^{cp} Russian Research Centre Kurchatov Institute, Moscow, Russia
- ^{cq} Saha Institute of Nuclear Physics, Kolkata, India
- ^{cr} School of Physics and Astronomy, University of Birmingham, Birmingham, United Kingdom
- ^{cs} Sección Física, Departamento de Ciencias, Pontificia Universidad Católica del Perú, Lima, Peru
- ^{ct} Sezione INFN, Bari, Italy
- ^{cu} Sezione INFN, Bologna, Italy
- ^{cv} Sezione INFN, Cagliari, Italy
- ^{cw} Sezione INFN, Catania, Italy
- ^{cx} Sezione INFN, Padova, Italy
- ^{cy} Sezione INFN, Rome, Italy
- ^{cz} Sezione INFN, Trieste, Italy
- ^{da} Sezione INFN, Turin, Italy
- ^{db} SSC IHEP of NRC Kurchatov Institute, Protvino, Russia
- ^{dc} SUBATECH, Ecole des Mines de Nantes, Université de Nantes, CNRS-IN2P3, Nantes, France
- ^{dd} Suranaree University of Technology, Nakhon Ratchasima, Thailand
- ^{de} Technical University of Split FESB, Split, Croatia
- ^{df} The Henryk Niewodniczanski Institute of Nuclear Physics, Polish Academy of Sciences, Cracow, Poland
- ^{dg} The University of Texas at Austin, Physics Department, Austin, TX, USA
- ^{dh} Universidad Autónoma de Sinaloa, Culiacán, Mexico
- ^{di} Universidade de São Paulo (USP), São Paulo, Brazil
- ^{dj} Universidade Estadual de Campinas (UNICAMP), Campinas, Brazil
- ^{dk} University of Houston, Houston, TX, United States
- ^{dl} University of Jyväskylä, Jyväskylä, Finland
- ^{dm} University of Liverpool, Liverpool, United Kingdom
- ^{dn} University of Tennessee, Knoxville, TN, United States
- ^{do} University of Tokyo, Tokyo, Japan
- ^{dp} University of Tsukuba, Tsukuba, Japan
- ^{dq} University of Zagreb, Zagreb, Croatia
- ^{dr} Université de Lyon, Université Lyon 1, CNRS/IN2P3, IPN-Lyon, Villeurbanne, France

^{ds} *V. Fock Institute for Physics, St. Petersburg State University, St. Petersburg, Russia*

^{dt} *Variable Energy Cyclotron Centre, Kolkata, India*

^{du} *Vestfold University College, Tonsberg, Norway*

^{dv} *Warsaw University of Technology, Warsaw, Poland*

^{dw} *Wayne State University, Detroit, MI, United States*

^{dx} *Wigner Research Centre for Physics, Hungarian Academy of Sciences, Budapest, Hungary*

^{dy} *Yale University, New Haven, CT, United States*

^{dz} *Yonsei University, Seoul, South Korea*

^{ea} *Zentrum für Technologietransfer und Telekommunikation (ZTT), Fachhochschule Worms, Worms, Germany*

¹ Also at: St. Petersburg State Polytechnical University.

² Deceased.

³ Also at: Department of Applied Physics, Aligarh Muslim University, Aligarh, India.

⁴ Also at: M.V. Lomonosov Moscow State University, D.V. Skobeltsyn Institute of Nuclear Physics, Moscow, Russia.

⁵ Also at: University of Belgrade, Faculty of Physics and “Vinča” Institute of Nuclear Sciences, Belgrade, Serbia.

⁶ Permanent Address: Konkuk University, Seoul, South Korea.

⁷ Also at: Institute of Theoretical Physics, University of Wrocław, Wrocław, Poland.

⁸ Also at: University of Kansas, Lawrence, KS, United States.